Lab on a Chip

PAPER

View Article Online
View Journal

Cite this: DOI: 10.1039/c6lc00968a

Universal microfluidic platform for bioassays in anchored droplets†

Gabriel Amselem,‡ Cyprien Guermonprez,‡ Benoît Drogue, Sébastien Michelin and Charles N. Baroud*

In spite of the large number of droplet-based microfluidic tools that have appeared in recent years, their penetration into non-specialist labs remains limited to a small number of applications. This is partly due to the lack of a generic platform that integrates all of the necessary operations for end-users, and partly to the increasing complexity that emerges as several operations are combined together. Here we report the development of a platform that provides the capabilities of multiwell plates in a two-dimensional array of nanoliter droplets: encapsulation, time-resolved monitoring and variation of well contents, as well as the ability to selectively extract the contents of any of the wells. We demonstrate these capabilities by encapsulating thousands of individual bacterial cells in droplets that are stored on a two-dimensional array of surface-energy anchors. Bacterial culture can be performed either in liquid or hydrogel droplets, both of which allow precise quantification using either standard measurements or digital enumeration. Using hydrogels allows the removal of the external oil that surrounds the aqueous drops, for instance in order to apply a gradient of antibiotics across the droplet population. This defines a protocol to obtain an antibiogram in a single experiment. Finally, the liquid to gel transition provides a robust way to selectively extract any droplet from the array, by melting it with a focused laser. When combined with further off-chip culture or genotyping, this platform provides a unique culturing environment to relate phenotype and genotype measurements on monoclonal colonies.

Received 29th July 2016,
Accepted 16th September 2016

DOI: 10.1039/c6lc00968a

www.rsc.org/loc

Introduction

In the early days of microfluidics, much effort was devoted to the development of new methods enabling elementary operations on a fluid sample. For example, in the area of droplet microfluidics, different methods of droplet production were invented in the early 2000s, from T-junction breakup[1] to capillary flow-focusing[2] and planar flow-focusing.[3] Beyond droplet production, various techniques of droplet sorting were also proposed, either by dielectrophoresis,[4] by optical means,[5] or through the use of surface acoustic waves,[6] in addition to methods for merging or breaking the drops, or mixing their contents.[7,8] Once the protocols for individual operations were established, they could be combined together to create platforms that integrated multiple operations. For example, a platform combining droplet production and sorting was used to perform directed evolution of enzymes, enabling the screening of libraries of $\sim 10^7$ enzymes and the selection of rare mutants with enhanced catalytic rates.[9] Such protocols are only possible through the use of microfluidics techniques, and the further development of microfluidics is expected to enable the emergence of other applications, in particular in the field of microbiology.

Nevertheless, the ubiquitous platform for quantitative measurements in biology labs remains the multiwell plate rather than microfluidic devices. In addition to its versatility and ease of use, the multiwell format features several key functionalities: (i) samples are isolated in their respective wells; (ii) the contents of each well can be monitored in time; (iii) the contents can be stimulated multiple times by pipetting further compounds into the wells; and (iv) the population from a singlewell can be retrieved at any time for further processing. To date, the two microfluidic systems that come closest to achieving this whole range of functionalities are single-phase, valve-based devices,[10] and electrowetting-on-dielectric (EWOD) chips.[11–13] Both valve-based and EWOD systems are programmable, which allows them to address a broad range of problems. This comes at the cost of a complex microfabrication processes, and an increasing complexity in the device manipulation when the number of reaction steps becomes large.

LadHyX and Department of Mechanics, Ecole Polytechnique, CNRS, 91128 Palaiseau, France. E-mail: baroud@ladhyx.polytechnique.fr

† Electronic supplementary information (ESI) available: Supplementary figure and movies. See DOI: 10.1039/c6lc00968a

‡ These authors contributed equally to this work.

There has recently been a rise in awareness to the importance of developing simpler microfluidic protocols, while maintaining a high standard on the device robustness.[14,15] In line with these preoccupations, one approach that has attracted broad attention is droplet microfluidics.[16–23] Compared with valve-based and EWOD devices, droplet microfluidic systems rely on easier microfabrication and are more suited to handling large numbers of reactions. Several droplet-based renditions of a multiwell plate have been proposed, in the form of static arrays of droplets. Many of these variations consist in designing quasi-2D geometries, where linear channels are connected to in-line or side pockets for droplet storage.[16,23–29] In other cases, droplets are stored in truly 2D chambers. These ensure a high degree of robustness since they are very tolerant to flaws or impurities. Indeed, in a linear channel the presence of a single defect or dust can block all downstream flow, while in a wide chamber the liquid simply flows around the impurity. In such 2D geometries, storage is performed either using traps[30,31] or simply by packing the droplets in large chambers.[32–34] In all cases, sample encapsulation and droplet monitoring are readily achieved. Yet, only a couple platforms allow the addition of a new stimulus to the encapsulated cells,[16,28,29] and none offer solutions for single-droplet retrieval.

Here, we present a novel droplet-microfluidic device covering the complete range of operations of a standard multiwell plate. The platform enables sample compartmentalization, monitoring, stimulus, and retrieval, while providing access to nearly 1500 independent experiments in parallel on a 2 cm^2 area. The device microfabrication and the platform operation were aimed to be as simple as possible. For this, we revisit the elementary methods of droplet-based microfluidics, from

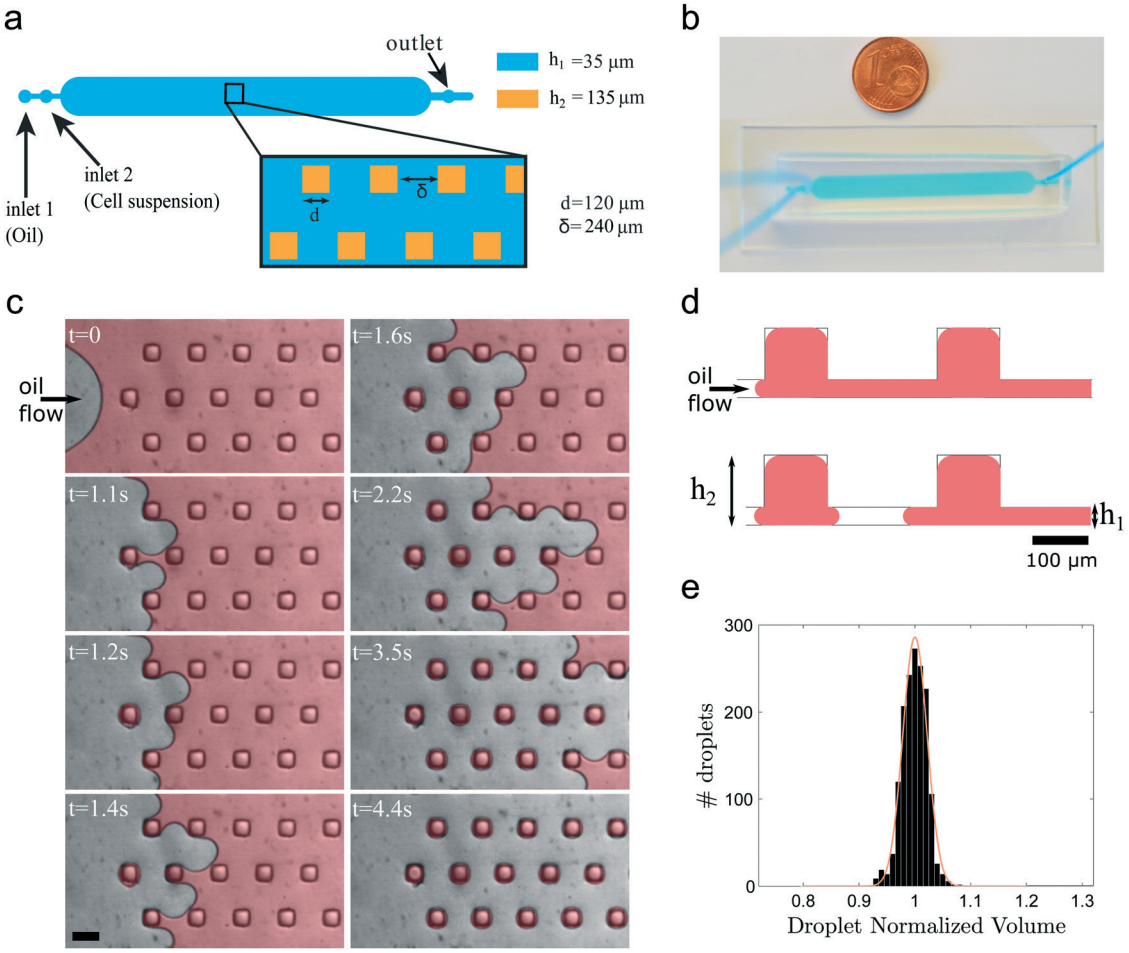

Fig. 1 Description of the microfluidic device and protocol for droplet production: (a) typical design of a microdroplet multiwell device. The central chamber has dimensions 0.5 × 4.8 cm and contains a 2D array of 115 × 13 surface-tension anchors. Square anchors have side dimension d = 120 μm, spaced by δ = 240 μm. The chamber height is h_1 = 35 μm and the anchor height h_2 = 135 μm. (b) The device, which fits on a microscope slide, is connected to two inlets and one outlet. (c) Time-lapse of the drop formation process. At t = 0, the cell sample fills the microfluidic chamber entirely, and is being pushed by fluorinated oil (FC40 + 0.5% surfactant) using a hand-pushed syringe. The arrow indicates the oil flow direction. When the interface penetrates between two anchors, it deforms and then breaks, which leaves a well-calibrated droplet in the anchor. The cell sample is coloured in red for better visualisation. Scale bar: 200 μm. (d) Cross-sectional schematic of the breaking process on anchors. The aqueous sample initially fills large regions and then gets divided into isolated droplets that fill each of the anchors. (e) Experimental histogram of the normalized droplet volumes on one chip. The orange line is the best Gaussian fit to the data, leading a standard deviation σ = 0.02.

droplet production and storage to droplet sorting. We introduce a novel way of creating a chemical gradient across the droplet array, and demonstrate the capacities of this device by culturing thousands of individual bacteria in parallel on a single chip, encapsulated in liquid or agarose droplets.

Results and discussion

Microfluidic device and protocol

The device developed here consists of a wide chamber with a 2D geometry, connected to two inlets and one outlet. An array of 1495 square indentations (anchors) was etched on the chamber ceiling, at a density of ~800 anchors cm^{-2}, see Fig. 1a and b. This geometry was chosen to provide regions of low confinement, within the anchors, surrounded by regions of high confinement. These "confinement gradients" allow the production of large forces, by providing local minima of the surface energy of the aqueous–oil interfaces.[35,36]

Before the beginning of an experiment, the whole device is rendered hydrophobic and filled with a fluorinated oil. The experiment begins when the aqueous cell suspension is injected into the device, forming a puddle of aqueous phase that fills the entire chamber. Then, fluorinated oil is flowed into the chip, pushing the cell suspension out of the chamber (Fig. 1c and Movie S1†). As the water–oil interface advances, some of the aqueous phase is trapped in each of the anchors. This deforms the puddle locally, until the geometry of the interface reaches a critical shape beyond which a droplet breaks off and remains in the low confinement region (Fig. 1d). Using an oil flow rate of 10 μL min^{-1}, droplets are created at 10 Hz, such that the whole chip is loaded within 3 minutes. Note that in contrast to our previous work,[21] where anchors were round, here we designed square-shaped anchors. This geometry allows the oil to drain out quicker of the anchors, due to the presence of corners.

Droplets formed by breaking up a large puddle on surface-energy anchors have a precisely controlled size. In our setup, droplets have a mean volume of 2 nL, with standard deviations ranging between 2% and 5% (see Fig. 1e for the droplet size distribution on one chip, and Fig. S1 and S2† for more data). The dispersion in droplet size varies slightly from chip to chip, and depends on the precision in microfabrication and on the quality of the hydrophobic surface treatment. The good monodispersity is due to the mechanism of break-up, detailed in ref. 21. Briefly, the aqueous puddle adapts its shape to minimize the surface energy in the channel. For small interface deformations, the puddle can find static equilibrium shapes. But as the oil pushes the interface further from the equilibrium position, the local shape forms thin necks that remain connected to the anchors. When these necks extend beyond a critical deformation, they cannot reach an equilibrium shape anymore, which causes them to break up and to leave a droplet in the anchor. This scenario takes place even for quasi-static motion of the interface and is mainly dependent on the device geometry. It is nearly independent of physical parameters – such as fluids viscosities, visco-elasticity, or surface tension – and of the velocity at which the oil phase is driven.[21] In a large chamber, droplet size heterogeneity is partly due to the flow-induced deformation of the PDMS. In our experiments, we found that using flow rates of 10 μL min^{-1} or lower led to satisfactory monodispersity.

Cell culture

In the rest of the article, we focus on droplets encapsulating bacteria with their appropriate growth medium. Bacterial proliferation within the droplets can easily be observed, as the drops remain immobile in their traps. Thus, the contents of each anchor can be imaged and re-visited at any time point.

Cells of a fluorescent strain of *Escherichia coli* (*E. coli* pGlo, expressing a plasmid encoded GFP with ampicillin resistance) are encapsulated in liquid droplets of LB broth to validate the microfluidic setup as a viable microbial culture platform. As in standard liquid cultures, cells grow in their planktonic state and are freely moving within the droplet. A time-lapse sequence of such a condition is shown in Fig. 2a (see Fig. S3† for an enlarged version). Each droplet plays the role of an independent, miniature liquid batch culture. In this operating mode, the device fills the functions of a high-density microwell plate, by allowing the parallelization of thousands of cultures, while guaranteeing continuous visual access to all of them.

The microfluidic device can also be used in a different manner, by working with droplets that mix low-gelling agarose with cells resuspended in growth medium. This mode mimics the way Petri dishes are used with an agar layer, for colony inspection, mutant isolation or cell enumeration. The protocol for breaking agarose droplets on the anchors is exactly the same as for liquid droplets, as the break-up process is not influenced by the physical properties of the fluids at play. Droplets are formed at room temperature, when agarose is in its liquid state. The immobilized agarose droplets are then gelled by placing the device at 4 °C for 30 minutes. After gelation, the microfluidic chip is placed in an incubator at 37 °C, a temperature that allows the bacteria to proliferate while the agarose droplets remain in their gel state. In gelled droplets, single *E. coli* bacteria grow to form compact 3D microcolonies, as shown in Fig. 2b, and can readily be observed in bright field and fluorescence imaging.

The 3D microcolonies formed by different bacterial species present different morphologies. As examples, we show in Fig. 2c monoclonal bacterial colonies from single *E. coli*, *Bacillus subtilis* and *Pseudomonas fluorescens* cells, after 16 hours of culture. While *E. coli* and *P. fluorescens* form compact round shaped micro-colonies, *B. subtilis* colonies develop in dendritic patterns. Colonies of *P. fluorescens* have a rough aspect and a lower optical density than colonies of *E. coli*. This visual inspection recalls the signature of different colonies on agar-coated Petri dishes, where colonies of different species may present different shapes, patterns and colors.

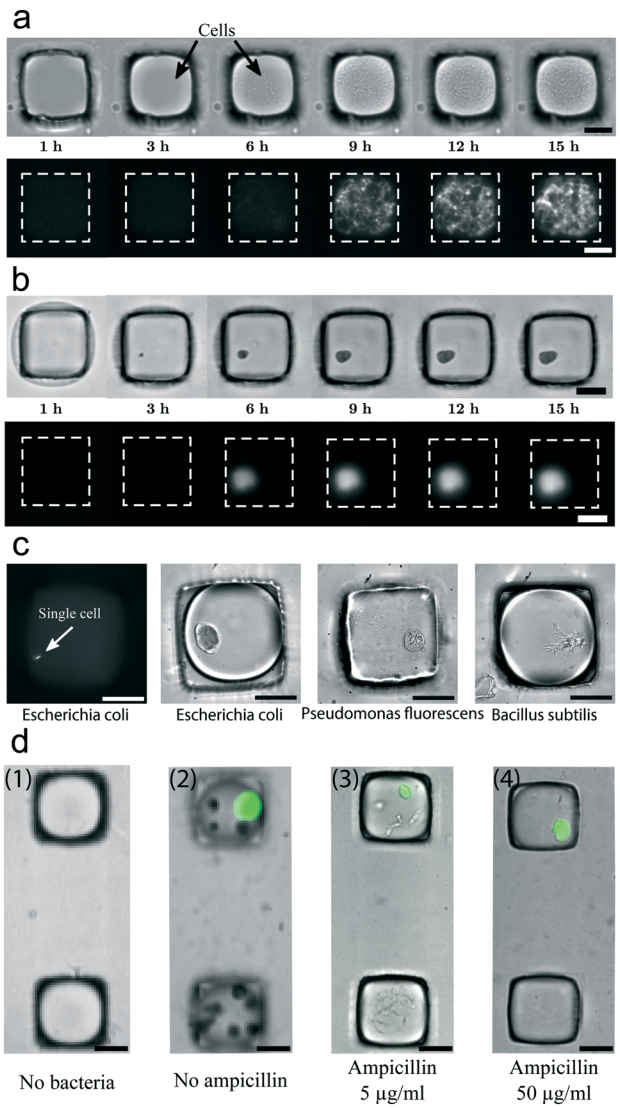

Fig. 2 Characteristic images of growth in different conditions: (a) growth of fluorescent *E. coli* pGlo mutants in a liquid droplet containing Luria-Bertani (LB) broth. Cells grow in their planktonic state and can move freely within the droplet. Top: Bright field image. Bottom: Fluorescence image. Scale bar: 50 μm. (b) When cultured in a gelled agarose droplet, the same bacteria grow as a 3D colony (see Movie S2†). Top: Bright field image. Bottom: Fluorescence image. Scale bar: 50 μm. (c) Left picture: Single *E. coli* pGlo bacterium, seeded in a gel droplet. Other pictures: after 16 hours of growth, three species of bacteria grow as 3D colonies with different shapes. (d) 3D colonies of WT (non-fluorescent) and pGlo mutants (fluorescent) co-encapsulated in gelled droplets. Images taken after 16 hours of growth. The initial ratio of WT : pGlo is always 100 : 1, and the amount of ampicillin in the droplets is varied. Panel 1: Test for external contamination. No colonies grow in the device when no bacteria are inoculated in droplets. Panel 2: Mutants and WT grow in the absence of ampicillin. Panel 3: In the presence of ampicillin at a concentration of 5 μg mL^{-1}, mutants form 3D colonies, while WT grow as filaments. Panel 4: When the concentration of ampicillin is increased to 50 μg mL^{-1}, only the mutants grow and form 3D colonies, while WT growth is suppressed. Scale bar: 50 μm.

In addition to cells and culture medium, the droplets can also contain any molecule of interest. As an example, *E. coli* pGlo (fluorescent) and WT (non-fluorescent) cells were co-encapsulated in gel droplets containing three concentrations of ampicillin (0, 5 or 50 μg ml^{-1}, Fig. 2d). In the absence of ampicillin, both WT and pGlo mutants grow as round shaped colonies (Fig. 2d-panel 2). At an ampicillin concentration of 5 μg ml^{-1}, cell growth of *E. coli* WT is impaired but not completely abolished, as shown by the small and filamentous shape of non-fluorescent WT colonies, typical of stressed bacteria. Under the same conditions, pGlo mutants still form round shaped micro-colonies, as their growth is not modified (Fig. 2d-panel 3). When the ampicillin concentration inside the droplet is set to 50 μg ml^{-1}, only mutants are able to grow (Fig. 2d-panel 4).

Enumeration methods

Apart from allowing species to be visually inspected, the microfluidic device extends the quantification capabilities of classical techniques in several important ways, both for enumerating the bacteria in a sample or for detecting rare events within a mix. Since the quantification hinges on the control of unwanted contaminations, we begin by testing the device robustness against contamination. This is confirmed since no micro-organisms are observed in the droplets, after 16 hours of incubation, when we do not specifically put bacteria in them (Fig. 2d-panel 1).

There are three ways of enumerating bacteria, which require different microscopy resolutions. When devices are inoculated, single bacteria can be observed under the microscope at a 40× magnification, as shown in Fig. 2c: detection of the droplet contents can take place without waiting for the colonies to grow. This mode of bacterial detection however requires high optical resolution, with access to length scales ~1 μm. To detect bacteria with lower (*e.g.* 10×) magnification objectives, enumeration can be carried out on bacterial micro-colonies after 10–20 hours of growth, see Fig. 2d-panel 2. Note that more than one bacterium per droplet can be encapsulated and still form distinguishable, independent micro-colonies. By seeding on average 7 cells per droplet, it is possible to detect a single mutant colony among more than 10 000 WT colonies. This is almost two orders of magnitude higher than what is currently achievable in a single Petri dish, where the threshold for mutant detection is of one mutant per 200 wild-type cells.[37]

The above methods are "analog": they are based on identifying and counting each encapsulated colony (or single cell) in order to estimate the initial cell concentration. Yet, the large number of wells available on the micro-chip also allows a "digital" approach to be used, and obtain quantitative measurements of the initial sample.[38] In this approach, the contents of each well are treated as a digital signal, *i.e.* either taking a one or zero value, depending on the presence or absence of signal of interest. This approach has been applied to the quantification of nucleic acids (digital PCR) and was shown to provide higher sensitivity and better quantification than analog techniques.[39]

The basic principle of a digital approach relies on the Poisson theory for finding a rare event in a random experiment. Assuming that cells are homogeneously distributed in the original suspension, that droplets are monodisperse, and that the number of cells in a given droplet is independent from the contents of other droplets, the distribution of the number of cells per droplet follows a Poisson law.[40] The probability of finding k colonies in a droplet is then given by:

$$\mathbb{P}(k) = \frac{\lambda^k}{k!} e^{-\lambda} \quad (k = 0, 1, \ldots), \tag{1}$$

where λ is the average number of colonies per droplet. The probability of having an empty droplet is therefore:

$$\mathbb{P}(0) = e^{-\lambda}, \tag{2}$$

which allows us to estimate the initial number of cells per droplet, $\hat{\lambda}$, by counting the fraction $\hat{p}_-$ of empty droplets on the chip:[40]

$$\hat{\lambda} \simeq -\ln(\hat{p}_-). \tag{3}$$

The 95% confidence interval on $\hat{\lambda}$ can likewise be estimated, see Material and methods. For the microfluidic device containing 1495 independent droplets of volume 2 nL, the range of concentrations that can be estimated with a relative error smaller than 20% spans two orders of magnitude, from $\sim 7 \times 10^4$ to $\sim 3 \times 10^6$ cells per mL.

We experimentally verify that the number of cells per droplet follows a Poisson distribution by counting the number of colonies in each solidified gel drop, as shown in Fig. 3a–c. The resulting distribution is fitted with a Poisson distribution using λ as the sole fitting parameter. We observe a good agreement between the measured and fitted distributions, which can be attributed to the weak physical interactions between bacteria during the loading process and to the good monodispersity of the compartment sizes in the chip.

As a proof of concept of the digital enumeration method, a sample of *E. coli* with an initial known concentration of 1 cell per nL is loaded on the device and scanned on a low-

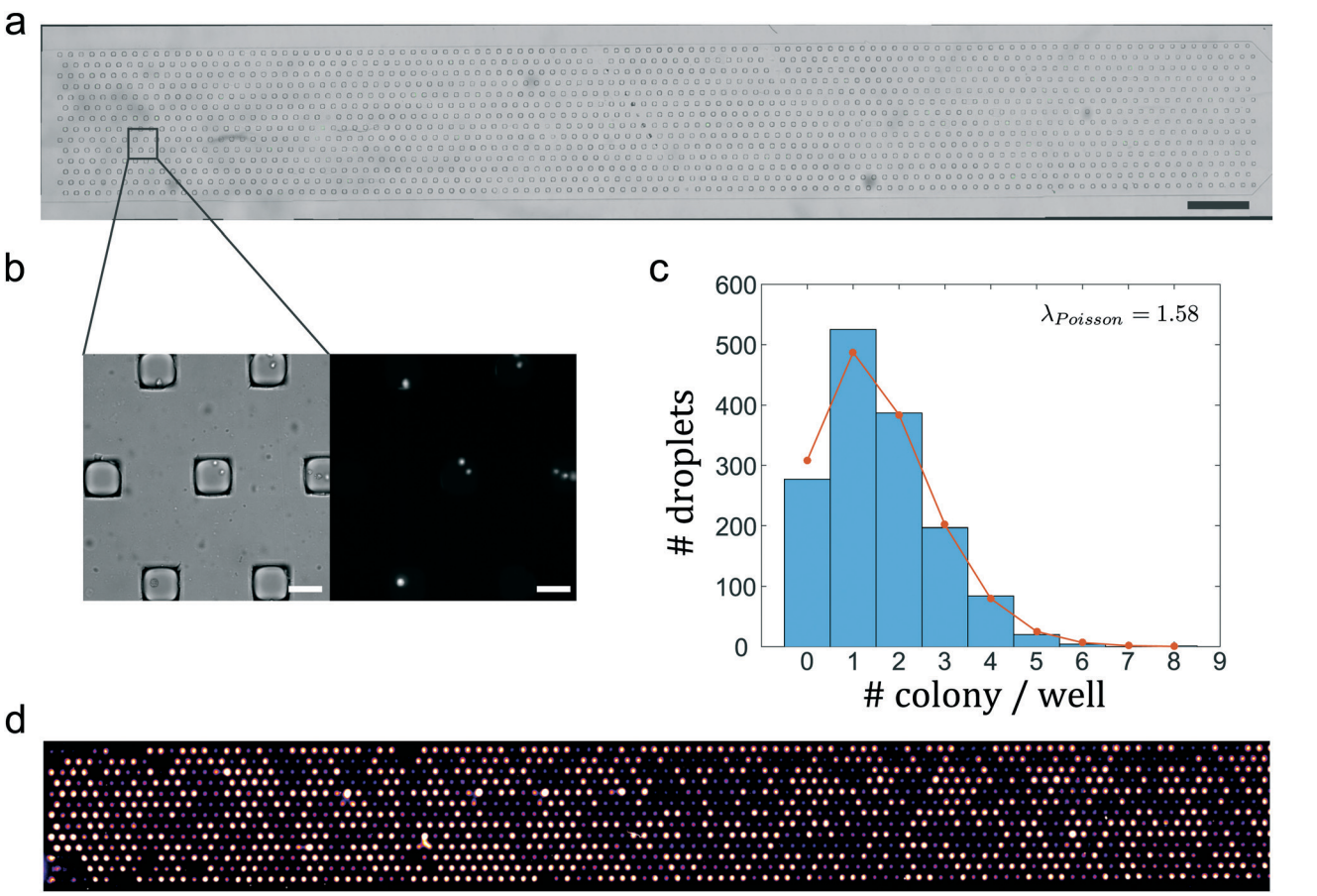

Fig. 3 Digital enumeration: (a) snapshot of the chip with 1495 individual droplets containing 3D colonies of fluorescent bacteria. Scale bar: 2 mm. (b) Zoomed view on the anchors, the droplets, and the encapsulated fluorescent 3D bacterial colonies. Left: Bright field image. Right: Fluorescence image. Scale bar: 100 μm. (c) Experimental distribution of the number of colonies per droplet (dots), and best fit to a Poisson distribution (bars). λ = 1.58 indicates that there are on average 1.58 cells per drop. (d) Low-resolution image taken on a slide scanner. A digital approach allows the concentration in the initial sample to be extracted from the number of positive droplets for a wide range of concentrations. Over the non-empty wells detected, we measured 941 positive and 135 negative droplets. Here, the estimated number of initial cells per droplet is $\hat{\lambda} \in [1.92; 2.25]$.

resolution slide scanner after 24 h incubation at 37 °C. We count $N_+ = 941$ positive anchors on the fluorescence image (Fig. 3d), and $N_- = 135$ empty droplets. This leads to an average initial number of bacteria per droplet and its associated 95% confidence interval of $\hat{\lambda} = 2.07 \pm 0.015$ cells per droplet (see Material and methods). The droplet volume being 2 nL, we indeed recover the expected concentration of cells in the initial sample, that is 1.0×10^6 cells per mL.

Compared with the direct visualisation of the colonies in each droplet, the digital approach simplifies the work flow by allowing us to work with lower resolution images, which makes them fast to acquire and analyse. Indeed, the slide scanner has a spatial resolution of 6.5 μm, which is sufficient to differentiate positive and negative droplets, although not sufficient to count the colonies within each drop. More importantly, this allows us to obtain a quantification of cells cultured in liquid medium, without requiring the gel to separate the different colonies within each drop.

Dynamic measurements of population growth

Finally, time-resolved measurements of colonies within the array provide the ability to make dynamical analysis on the droplet contents. As an example, we show how the platform can be used to extract growth parameters of bacterial colonies. As shown in Fig. 4, nearly 1000 fluorescent monoclonal colonies of *B. subtilis* in liquid droplets are monitored over time by scanning the entire chip every 30 minutes on a motorized microscope (also see Movie S2†). The total fluorescence intensity is measured in each droplet as a proxy for the total number of bacteria in the drop, leading to the growth curves shown in Fig. 4a. In this figure, each green curve represents the evolution of the total fluorescence intensity of a single droplet, the thick blue curve shows the average behaviour at each time step, and black curves highlight randomly chosen example traces. Droplets where no fluorescence is detected are not shown in the figure. We observe a variability in final colony sizes as well as in the growth dynamics, which contrasts with the classical batch culture in which only the average behaviour would be detected.

We determine the usual bacterial growth parameters[41] to quantify the variability: the final colony size, corresponding to the fluorescence level of the drop after it reached a stationary phase; the lag time t_{lag}, period during which no growth is observed due to the adaptation time to the new environment, and to the fluorescence level being below the detection threshold;[42] the maximum growth rate g, which is the maximum slope of the growth curve; the specific growth rate $\mu_{\max}$, corresponding to the maximum value of the logarithmic growth rate; and the doubling time $\tau = \ln 2/\mu_{\max}$. For more details on the definition of growth parameters, see Materials and methods.

As shown in Fig. 4b, the values of each parameter are distributed around a well-defined peak. The spreading in each distribution highlights the inherent stochasticity in bacterial growth. The device thus allows to observe the dispersion of growth behaviours and in particular to detect events falling in the tails of the distribution, which would be hidden in classical batch measurement. All distributions are unimodal and no sub-populations can be detected, implying that the initial number of bacterial cells per droplet – ranging from 1 to 7 cells per droplet – does not appear to influence the

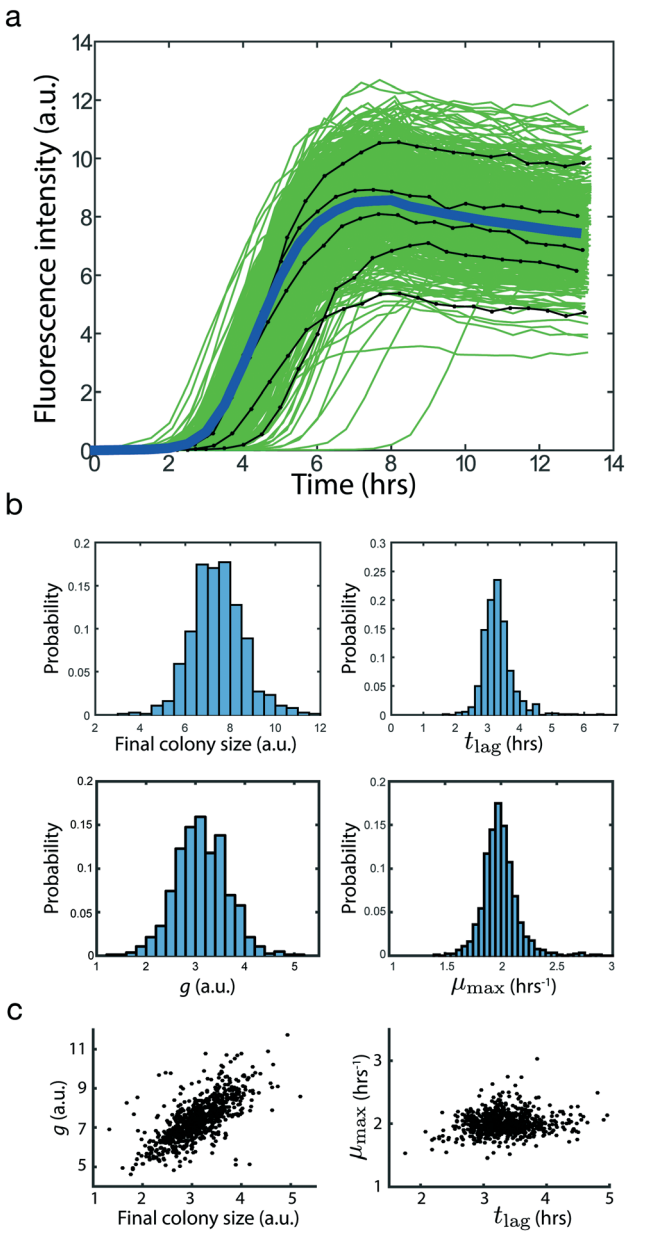

Fig. 4 Growth curve statistics: (a) growth of *B. subtilis* colonies monitored by fluorescence in 848 independent liquid droplets. Points are taken every 30 min. Five random black curves are highlighted for better reading. The thick blue curve corresponds to the mean intensity at each time step. (b) Histograms of four parameters characterizing bacterial growth: final colony size, lag time t_{lag}, maximum growth rate g and specific growth rate $\mu_{\max}$. (c) We find a strong correlation between the maximal growth rate g and the final colony size, but no correlation between other parameters, such as $\mu_{\max}$ *vs.* t_{lag}. Other figures showing the absence of correlation between parameters can be found in the ESI.†

growth behaviour. Parameter values measured in our device are similar to the ones measured in batch, indicating that the device does not induce any change in the growth behaviour of the bacterial culture (see Table 1).

Tracking individual growth curves enables to determine correlations – or lack thereof – between the growth parameters, an important knowledge for building models of bacterial growth. The data we recorded show that the lag time has no influence on the specific growth rate μ_{max}, the maximum growth rate g, or on the final colony size (see Fig. 4c and Fig. S4†). The only strong correlation we find is between g and the final colony size, see Fig. 4c. There is no correlation between the specific growth rate μ_{max} and the final colony size (Fig. S4†).

On-chip antibiogram

Much of the interest in performing parallel experiments using traditional multiwell plates lies in the ability to impose different conditions in each well. Several approaches can be explored to produce variable contents within the droplets. Here, we show how to produce an antibiotic gradient in the chip, which allows us to determine the *minimum inhibitory concentration* (MIC), at which all cells are killed, in a single experiment.

Generating a gradient in the microfluidic chip requires two modifications to the above experimental protocol. First, a double inlet distribution channel is added to one end of the chamber (see Methods, Fig. 8 and Fig. S5†).By forcing two solutions to flow side by side into the distribution channel, a gradient of concentration is produced, as described in detail in ref. 43. Second, a phase switch is performed, *i.e.* we replace the oil surrounding the anchored gel droplets with an aqueous phase, after gelation has occurred. During the phase switch, gelled droplets remain anchored due to the gel's elasticity, and water-soluble molecules present in the aqueous phase diffuse into the gel beads, eventually reaching the cells.

Then, in order to perform an antibiogram, the chip is loaded with an *E. coli* suspension as previously, and droplets are gelled within the anchors. Afterwards, a co-flow of LB culture medium and of LB with the drug gentamycin (c = 25 μg mL^{-1}) is imposed, replacing the oil phase. A gradient of gentamycin establishes across the width of the microfluidic chamber, with drug concentrations ranging between zero and 21 μg mL^{-1} for this particular geometry. Maintaining constant flows of LB and LB with gentamycin ensures that the antibiotic gradient is stable and each row of the 2D array is exposed to a constant concentration, see Fig. S5.† After 4 hours of gradient exposition, the chamber is washed with pure LB culture medium. Then, the aqueous phase is replaced by a new oil phase, thereby re-encapsulating the hydrogel droplets and preventing communication between them. The device is incubated at 37 °C for one day, after which it is imaged on a slide scanner, see Fig. 5a.

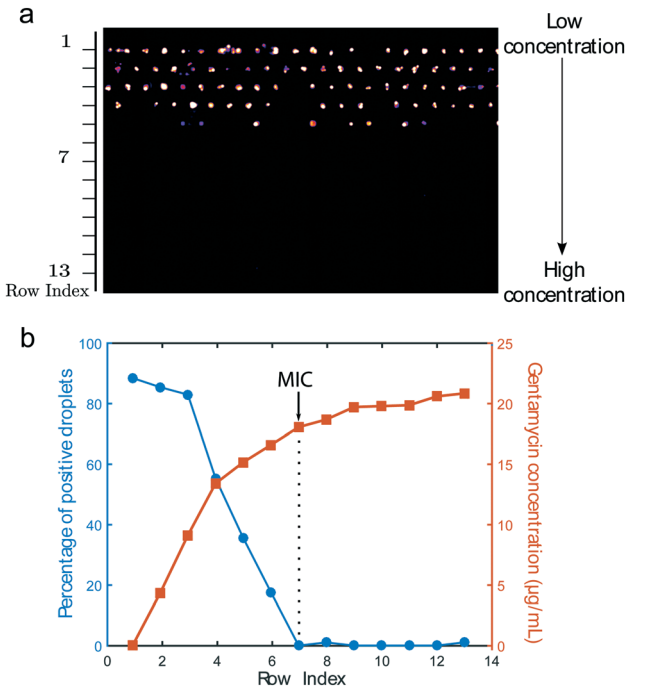

Fig. 5 On-chip antibiogram: (a) zoom on the microfluidic chip. Fluorescence signal after 4 h exposure of an *E. coli* culture to a concentration gradient of gentamycin, and two days of culture in LB medium without antibiotic at 37 °C. The lower part of the chip corresponds to the high antibiotic concentration region while the upper part is the low concentration region. Cells on a given row on the chip are exposed to the same, well-defined drug concentration. (b) Gentamycin concentration (orange squares, right y-axis), and percentage of droplets where *E. coli* grow (blue circles, left y-axis), as a function of the row number.

The concentration profile of gentamycin is plotted in Fig. 5b as a function of the well position in the chamber. Our two-dimensional array of anchors consists of 13 rows and 115 columns, so that 13 different drug conditions can be probed on the chip, and each condition is repeated 115 times. The percentage of surviving cells, as determined by fluorescence, is shown in the same graph for each drug concentration. The number of survivors starts to decrease for concentration greater than 9 μg mL^{-1}, and no cells survive for concentrations larger than 17 μg mL^{-1}, which defines the MIC for this bacterial strain in this conditions.

Table 1 Comparison between the measurements of lag times (t_{lag}), doubling times (τ) and specific growth rates (μ_{max}) for culture on device and batch culture. For on chip culture, the mean values of each parameter are given with an error corresponding to the standard deviation of the data set (Fig. 4b)

Data set	State	t_{lag} (h)	τ (min)	μ_{max} (h^{-1})
Device	Liquid	3.37 ± 0.68	21 ± 2	2.01 ± 0.18
Batch	Liquid	~2	30	1.38

Extraction of individual colonies

A recurring desire of microbiologists is to be able to extract a single droplet from the array for further culture or analysis.

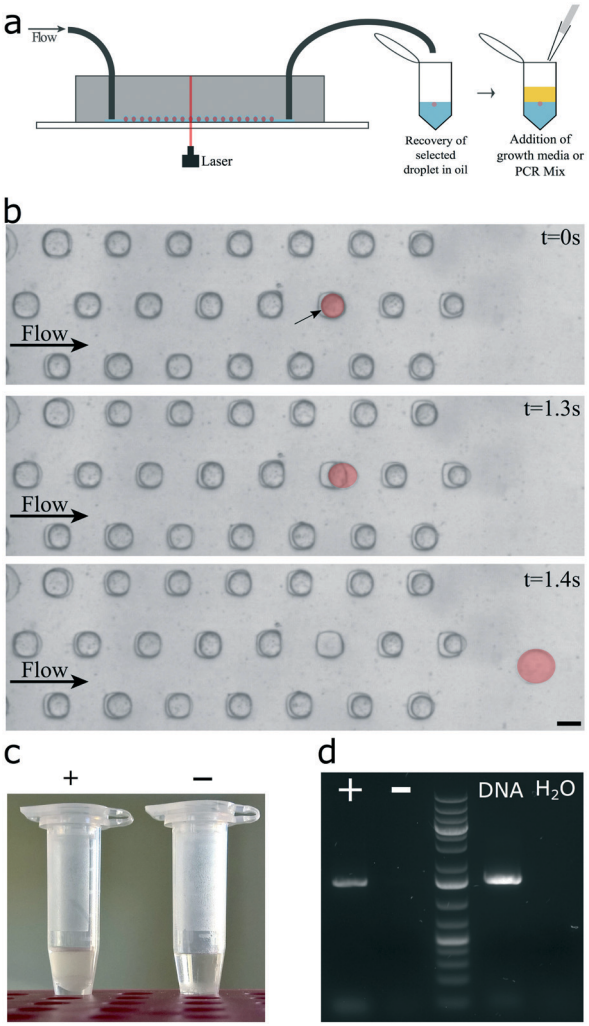

Fig. 6 Selective droplet extraction: the desired droplet is liquefied using an infrared laser, and a flow of oil is applied. This leads to the untrapping of the selected droplet, while all other droplets, still gelled, are stuck in their traps. The liquid droplet is recovered with oil in an eppendorf tube at the exit of the microfluidic device. (a) Sketch of the setup. (b) Snapshots of the droplet recovery. The droplet indicated by an arrow and colored in red for better visualization has been liquefied using the laser. At t = 0, a flow of 280 μL min^{-1} is imposed. Scale bar, 200 μm. (c) After overnight incubation, bacteria have grown in tubes where bacteria-filled droplets were recovered (+), not in tubes where empty droplets were recovered (–). (d) Droplet contents can be amplified. DNA from a single bacteria-filled droplet (+) are detected on the gel and not from empty droplets (–).

This operation is particularly difficult in most microfluidic approaches and remains a blocking point for the adoption of microfluidics by biologists. Here we take advantage of our 2D geometry to selectively recover individual droplets out of the chip, since extracting a single droplet from the array does not disturb the rest of the anchored drops.

The extraction protocol relies on selectively melting an individual agarose droplet by heating it with a focused laser. The infrared laser is directed through the microscope objective to a spot size of around 2 μm and can be positioned at any location within the field of view of the microscope (see methods for detailed setup). Therefore by focusing the laser spot within a particular droplet for a few seconds, the agarose is melted only within the chosen drop. Then by imposing an oil flow beyond a critical value of 280 μL min^{-1}, the liquid droplet is pushed outside of its trap and recovered in a microcentrifuge tube outside of the device, as shown in Fig. 6 and Movie S3.† In contrast with the work reported by Fradet *et al.*,[44] the anchor dimensions and the difference in rigidity between liquid and gel drops here makes the recovery process robust and fast. During this process all the gelled droplets remain immobilized inside the chip, rigidly constrained in their respective traps. The protocol can be repeated to recover as many droplets as needed out of the chip. To ensure that no cross contamination occurs during retrieval, a washing step with oil is generally performed between each droplet recovery.

As a proof of concept, a chip with agarose droplets encapsulating pGlo mutants is incubated overnight, such that bacteria form individual colonies. Then, a droplet containing a colony is recovered in a microcentrifuge tube, along with the oil used to extract it. From this step on, two different paths are explored: either the extracted bacteria are subcultured, or a polymerase chain reaction (PCR) is performed. For subculturing, LB broth is added to all tubes containing a single droplet and samples are incubated two days at 37 °C under agitation. Bacterial growth of the expected strain was observed only for droplets containing a microcolony, see Fig. 6c. This result indicates that the retrieval process does not alter the viability of the extracted cells. For PCR amplification on the recovered droplets, the expected amplicon was detected for positive samples (tubes containing a single positive droplet), while no DNA fragment was amplified for negative droplets, see Fig. 6d. Even though further optimizations are needed to reduce the risk of cross-contaminations, the universal microfluidic platform is the first device enabling such a wide range of high-throughput phenotypic measurements that can be directly correlated to genotypic analyses out of the chip.

Conclusion

As the field of microfluidics matures, a large number of basic operations have become available, such as droplet production, sorting, splitting, or merging for example. These basic operations are then combined together to create platforms that integrate several operations into a coherent device for a range of applications. Here we present a microfluidic platform that is unique in several important respects. First, it is highly versatile and allows a wide range of manipulations and measurements to be performed. Second it allows a large number of time-dependent observations and manipulations to be run in parallel, either in order to explore the inherent variability of biological samples, *e.g.* when working on the single-cell level, or by applying variable forcing on the cells. Third, it allows the selective recovery of any one of the droplets for further culture or analysis. Finally and most

importantly, the microfluidic device is very simple to fabricate and to use, which will favor its adoption beyond the field of microfluidics.

The capabilities of this platform are demonstrated in the case of bacterial culture and manipulation. We show that bacterial cells can be encapsulated into nL-scale droplets and cultured for several days, while having direct visual access to the contents of each droplet at all times (Fig. 2). This enables different analysis methods to be implemented, either by detecting individual cells or colonies, or by making integrated measurements at the scale of an anchor (Fig. 3). The geometric approach to droplet production *in situ* (Fig. 1) ensures reproducible droplet production even if the rheological properties of the aqueous solution are varied. This has allowed the same protocols to be employed with gel solutions that can later be solidified. This phase change provides several added functionalities, such as the ability to bring external stimuli to the sample by replacing the oil phase with an aqueous phase (Fig. 5), or the ability to extract any droplet from the two-dimensional array by selectively melting it and pushing it out with the external flow (Fig. 6).

The platform presented here is generic: it is not tailored to address a particular biological problem but provides instead a novel approach to perform microfluidics generally. Although there exist microfluidic designs that allow the individual elementary operations enabled by our device, the integration of droplet production, storage, changing the droplet contents and droplet recovery in a single device has not been showcased with current techniques. Yet, these operations are critical for biology protocols and constitute the microfluidic counterparts of the functionalities fulfilled by multiwell plates. This will provide opportunities for a variety of biological applications, from drug screening to antibody production to unravelling interactions between co-cultured bacterial strains. Furthermore, recovering previously monitored droplets and performing a whole genome amplification on their contents will directly link a cellular phenotype to its genotype.

Material and methods

Microfluidic device

The microfluidic chip consists in a 2D chamber of height h_1 = 35 μm, with two inlets and one outlet, see Fig. 1a. The chamber ceiling is patterned with a 2D array of grooves (or "anchors") of typical size d = 120 μm and height h_2 = 135 μm. Space between the anchors was set to δ = 240 μm.

Molds were made using the dry-photoresist process described in Fradet *et al.*[44] First, a photoresist layer of height h = 35 μm (Eternal Laminar) was laminated onto a clean glass coverslip, using an office laminator (PEAK PS320) set at 100 °C, and exposed to UV (Hamamatsu Lightningcure LC8) through a photomask to obtain the desired microfluidic chamber design. Then, two photoresist layers of height 50 μm were laminated on the top of the first layer and exposed to UV through a mask with the design of the 2D array of traps. Last, the mold was developed in a bath of water containing 1% (w/w) of carbonate potassium (Sigma-Aldrich). All microfluidic chips were molded in polydimethylsiloxane (PDMS, Dow-Corning Sylgard 184).

Once cured, PDMS chips were sealed to glass coverslips by plasma bonding. The chips were rendered hydrophobic by surface treatment with an electronic coating EG-1720 (Acota Ltd, Knights Way, Shrewsbury, UK): the microfluidic devices were filled with the solution and heated at 110 °C for 30 minutes. Surface treatment was repeated 3 times to ensure efficient hydrophobicity.

Droplet formation

For droplet formation, a first syringe (SGE–R Analytical Technologies, 1 mL) containing fluorinated oil (FC-40, 3M Fluoroinert) with 0.5% (w/w) pegylated surfactant (008-FluoroSurfactant, RAN Biotechnologies) was connected to inlet 1 of the microfluidic device. A second syringe (SGE–R Analytical Technologies, 100 μL) containing the cell suspension in 1.5% (w/w) low-gelling agarose (Agarose Type IX, Sigma-Aldrich) was connected to inlet 2, see Fig. 1a. The process of droplet formation comprises 3 steps: (i) the chamber is first entirely filled with oil; (ii) the oil flow is stopped and the cell sample is flown in at a flow rate of 10 μL min^{-1}, eventually entirely filling the microfluidic chamber; and (iii) the cell sample flow is stopped and a flow of oil pushes the cell sample towards the exit at a flow rate that increases between 10 and 50 μL min^{-1}, creating droplets of the cell sample immobilised on each trap, see Fig. 1c and 3a, and Movie S1.†

The microfluidic chip was then immersed into a water bath to prevent evaporation, and incubated at 37 °C for the duration of the experiment. In the case of agarose droplets, an additional step was required prior to incubation: the chip was placed at 4 °C during 30 minutes to ensure agarose gelation. After 16 hours at 37 °C, a very conservative estimate of the droplet average volume change shows a 12% decrease in volume, with more than 80% of droplets showing less than a 4% decrease in volume.

Bacterial strains, growth and PCR conditions

Three bacterial strains were grown in our device: *Bacillus subtilis* GM2919,[45] *Escherichia coli* HB101 K-12 (pGLO™ Bacterial Transformation Kit, Biorad) and *Pseudomonas fluorescens* F113 (a kind gift of Claire Prigent-Combaret and Sebastien Renoud, UMR 5557, Ecologie Microbienne Lyon). Cells were grown overnight (180 r.p.m.) in an incubator set at 28 °C for *P. fluorescens* and at 37 °C for *E. coli* and *B. subtilis*. Luria-Bertani (LB) medium was supplemented with arabinose 0.2% for *E. coli* and the relevant antibiotic as follows: gentamycin 25 μg mL^{-1} (*P. fluorescens*), spectinomycin 100 μg mL^{-1} (*B. subtilis*), ampicillin 100 μg mL^{-1} (*E. coli*). Cell cultures were harvested in late exponential phase and resuspended to a concentration of 1.0×10^6 cells per mL or 1.0×10^7 cells per mL, depending on the number of cells expected per droplets. 15 μL of the cell suspension were

mixed with 15 μL of sterile water for liquid droplets, or with 15 μL of a 3% (w/w) low-melting agarose solution for gel droplets.

Dynamic measurements of bacterial growth in droplets were made on the *B. subtilis* GM2919 strain, which has its fluorescence gene directly integrated in the genome.

PCR amplifications of 16S rRNA genes of *E. coli* strain were done according to the Taq polymerase manufacturer (New England Biolabs, Ipswich, MA) in 25 μL using the 1492r (5′-TACCTTGTTACGACTT) and the 27f (5′-AGAGTTTGATCCTGGCTCAG) primers. The amplification cycle consisted in initial step of 5 min at 98 °C; 35 cycles of 10 s at 98 °C, 15 s at 55 °C and 1 min at 72 °C; followed by a final elongation step of 2 min at 72 °C. Extracted droplets were resuspended in 10 μL of sterile water and 5 μL of the suspension were used as PCR sample.

Microscopy and laser setup

The microfluidic chip was analyzed with a Nikon Eclipse Ti-U microscope, equipped with a motorized *XYZ* stage, using an EM-CCD (Andor Technologies) and the accompanying NIS software. The motorisation enabled large scans of the entire chip with a 10× magnification (see Fig. 3a). Both bright field and fluorescence images were taken at each *XY* position (see Fig. 3a enlargement). A focus surface was programmed by the NIS software to set the focus on droplets median plan for each position.

To liquefy the agarose droplets of interest, a continuous infrared laser at λ = 1480 nm (Fitel Furukawa FOL1424) was mounted on a Nikon TE2000 microscope, such that the laser beam passes through the microscope's objective, as described in Cordero *et al.*[46] The laser position on the microfluidic chip was adjusted in real-time using 2 galvanometric mirrors (Cambridge Technologies 6210H), controlled by a custom-made LabView program.

Image analysis

For fluorescence measurements, the fluorescence signal is integrated on the entire image to ensure no signal loss. Fig. S6† shows the integrated signal as a function of the *z*-focus. As seen on the figure, fluorescent measurement does not vary by more than 2%, confirming that not being perfectly in focus for each drop does not lead to any loss of information.

The raw data consist in brightfield and fluorescence images, with each field of view containing multiple anchors (see Fig. 3(b)). A custom-made MATLAB program processes the images to follow bacteria growth. Individual wells are detected using bright-field images, and their fluorescence content is integrated, allowing for growth curves to be plotted (Fig. 4).

Cell enumeration

Counting the number of cells in a device (Petri dish or microfluidic chip) enables to estimate the concentration of cells in an original sample. When N cells are counted in a device, the width of the 95% confidence interval on N scales as $\sqrt{N}$. The relative precision of the measure therefore scales as $\sqrt{N}/N = 1/\sqrt{N}$: counting a larger number of cells leads to a better precision. In the device, a very conservative estimate of the largest initial number of cells per droplet leading to the growth of spatially segregated, individual colonies, was of the order of 5 cells per droplet, *i.e.* more than 7500 cells total. This is almost 100 times more than what can be grown on a Petri dish, so that the precision on N is about 10 times better in the microfluidic chip than in a Petri dish. Moreover, when using Petri dishes to estimate an unknown concentration from a sample, the sample is serially diluted with the aim to obtain a Petri dish with typically 10 to 200 individual cells, leading to the growth of 10 to 200 colonies. The dynamical range allowing for an estimation of the concentration is therefore of 1 order of magnitude in traditional settings. In the microfluidic device, this dynamical range was enhanced by one to two orders of magnitude, since the device could contain up to 7500 colonies.

Digital enumeration

For digital enumeration, the microfluidic chip was placed on a fluorescence slide-scanner (SensoSpot®-Fluorescence, Sensovation AG, Germany). By knowing the number of empty droplets, the Poisson theory enables us to estimate the initial number n_0 of bacteria cells per droplet. Let us define p_k the probability that $n_0 = k$. As p_k follows a Poisson distribution, we have:

$$p_k = \mathbb{P}(n_0 = k) = \frac{\lambda^k}{k!}\mathrm{e}^{-\lambda} \quad (0,1,\ldots) \tag{4}$$

with λ the expected value for n_0. λ depends on the initial cells concentration in the initial sample c_0 and the mean droplet volume v_d: $\lambda = c_0 v_d$.

The experimental ratio $\hat{p} = \frac{N_+}{N_+ + N_-}$ of positive drops to the total number of drops is used to build an estimator $\hat{\lambda}$ of λ, for the initial sample cells distribution within the droplets. By noticing that $\hat{p} = 1 - p_0$, one can deduce:

$$\hat{\lambda} \simeq -\ln(1 - \hat{p}) \tag{5}$$

The error made by taking $\hat{\lambda}$ instead of λ can be evaluated statistically. The 95% confidence interval of the real ratio of positive drops to the total number is $[p_{\min}, p_{\max}] = [\hat{p} - 1.96\sigma_{\hat{p}}, \hat{p} + 1.96\sigma_{\hat{p}}]$, with $\sigma_{\hat{p}} = \sqrt{\frac{\hat{p}(1-\hat{p})}{n_d}}$ the standard deviation of $\hat{p}$.[40] Thus, from this interval and eqn (5) we can calculate our 95% confidence interval on λ.

Growth curve analysis

For each experiment, five characteristic parameters are extracted from the bacterial growth curves (Fig. 4): the final

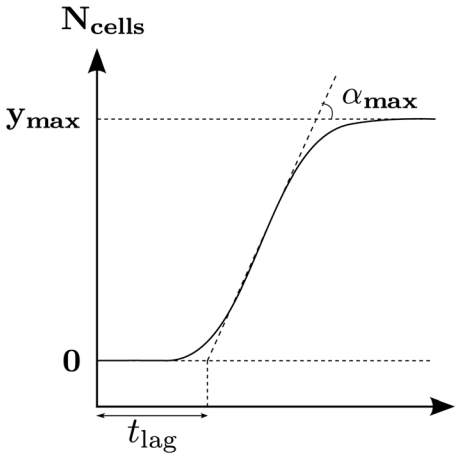

Fig. 7 Bacterial growth parameters: final colony size y_{max}, maximum growth rate $g = \tan \alpha_{max}$, lag time t_{lag}.

fluorescence level (or colonies sizes) y_{max}, the lag time t_{lag}, the maximum growth rate g, the specific growth rate μ_{max} and the doubling time τ. Fig. 7 shows the methods to perform the measurements.

The maximum growth rate is the maximum slope of the growth curve:

$$g = \max\left(\frac{dy}{dt}\right) = \tan \alpha_{max}. \quad (6)$$

The lag time is the duration of the lag phase. In practice, it is defined as the intersection between the tangent at the maximum exponential growth phase with the x-axis:[41]

$$t_{lag} = t_{max} - \frac{y_0}{\tan \alpha_{max}}. \quad (7)$$

The specific growth rate is typically define as the maximum rate of the logarithm of the growth curve:[47]

$$\mu_{max} = \max\left(\frac{d\ln y}{dt}\right) = \max\left(\frac{1}{y}\frac{dy}{dt}\right) \quad (8)$$

The doubling time corresponds to time required to double the fluorescent intensity during the maximum exponential growth phase:

$$\tau = \frac{\ln 2}{\mu_{max}} \quad (9)$$

Antibiogram

Implementing the antibiogram requires minor chip modifications. The outlet part is replaced by a distribution channel perpendicular to the main chamber, see Fig. 8. After droplet breaking and gelation using the standard protocol, the oil phase is replaced by an aqueous phase. A co-flow of LB broth and LB broth with gentamycin (25 μg mL^{-1}) is flowed at 2 × 3 μL min^{-1} through inlets 3 and 4, resulting in a L continuous concentration gradient orthogonally to the flow direction[43] with concentration ranging from 0 to 21 μg mL^{-1}. Each row experiences a well-defined antibiotic concentration, as presented on Fig. 5. The calibration for the gentamicin concentration has been prior made with fluorescein in the same chip. As the fluorescein and the gentamicin present a similar structure, it has been assumed that they have the same diffusion coefficient. As the Péclet number is over 400, the gentamycin does not transversally diffuses more than 27% of the distance between 2 anchors during its flow through the chamber. It ensures the constant concentration along each row. The gradient is maintained for 4 hours within the chambers, before rinsing the remaining antibiotic with LB broth. The aqueous phase is finally replaced with oil and the chip incubated at 37 °C to observe survivors.

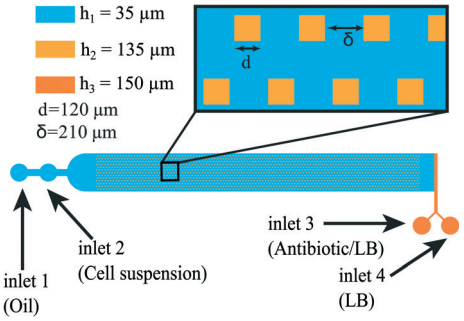

Fig. 8 General chip geometry for the production of a continuous concentration gradient within the chip. As in Fig. 1, inlets 1 and 2 are used for breaking the droplets on the anchors. The modification relies on the addition of inlets 3 and 4, which are used to produce the antibiotic concentration gradient.[43]

Acknowledgements

The research leading to these results received funding from the European Research Council (ERC) Grant Agreement 278248 Multicell. We would like to thank Caroline Frot for help with the microfabrication, Antoine Barizien and Charles Fosseprez. We are grateful to Claire Prigent-Combaret (CNRS UMR5557, Ecologie Microbienne, Lyon) and Dominique Le Coq (INRA UMR1319, Institut Micalis, Jouy-en-Josas) for gift of bacterial strains. PCR were done with the help of Roxane Lestini at CNRS UMR7645 (Laboratoire d'Optique et Biosciences, Palaiseau).

References

1 T. Thorsen, R. W. Roberts, F. H. Arnold and S. R. Quake, *Phys. Rev. Lett.*, 2001, **86**, 4163–4166.
2 A. M. Gañán-Calvo and J. M. Gordillo, *Phys. Rev. Lett.*, 2001, **87**, 274501.
3 S. L. Anna, N. Bontoux and H. A. Stone, *Appl. Phys. Lett.*, 2003, **82**, 364.

4 K. Ahn, C. Kerbage, T. Hynt, R. Westervelt, D. Link and D. Weitz, *Appl. Phys. Lett.*, 2006, **88**, 024104.
5 M. L. Cordero, D. R. Burnham, C. N. Baroud and D. McGloin, *Appl. Phys. Lett.*, 2008, **93**, 034107.
6 T. Franke, A. R. Abate, D. A. Weitz and A. Wixforth, *Lab Chip*, 2009, **9**, 2625.
7 C. Baroud, F. Gallaire and R. Dangla, *Lab Chip*, 2010, **10**, 2032–2045.
8 R. Seemann, M. Brinkmann, T. Pfohl and S. Herminghaus, *Rep. Prog. Phys.*, 2012, **75**, 016601.
9 J. J. Agresti, E. Antipov, A. R. Abate, K. Ahn, A. C. Rowat, J.-C. Baret, M. Marquez, A. M. Klibanov, A. D. Griffiths and D. A. Weitz, *Proc. Natl. Acad. Sci. U. S. A.*, 2010, **107**, 4004–4009.
10 T. Thorsen, S. J. Maerkl and S. R. Quake, *Science*, 2002, **298**, 580–584.
11 M. G. Pollack, R. B. Fair and A. D. Shenderov, *Appl. Phys. Lett.*, 2000, **77**, 1725.
12 S. K. Cho, H. Moon and C. J. Kim, *J. Microelectromech. Syst.*, 2003, **12**, 70–80.
13 M. Abdelgawad and A. R. Wheeler, *Adv. Mater.*, 2009, **21**, 920–925.
14 E. K. Sackmann, A. L. Fulton and D. J. Beebe, *Nature*, 2014, **507**, 181–189.
15 T. S. Kaminski, O. Scheler and P. Garstecki, *Lab Chip*, 2016, **16**, 2168–2187.
16 P. M. Korczyk, L. Derzsi, S. Jakiela and P. Garstecki, *Lab Chip*, 2013, 1–7.
17 J. E. Kreutz, T. Munson, T. Huynh, F. Shen, W. Du and R. F. Ismagilov, *Anal. Chem.*, 2011, **83**, 8158–8168.
18 T. Schneider, G. S. Yen, A. M. Thompson, D. R. Burnham and D. T. Chiu, *Anal. Chem.*, 2013, **85**, 10417–10423.
19 B. P. Casavant, E. Berthier, A. B. Theberge, J. Berthier, S. I. Montanez-Sauri, L. L. Bischel, K. Brakke, C. J. Hedman, W. Bushman, N. P. Keller and D. J. Beebe, *Proc. Natl. Acad. Sci. U. S. A.*, 2013, **110**, 10111–10116.
20 R. Dangla, S. C. Kayi and C. N. Baroud, *Proc. Natl. Acad. Sci. U. S. A.*, 2013, **110**, 853–858.
21 G. Amselem, P. T. Brun, F. Gallaire and C. N. Baroud, *Phys. Rev. Appl.*, 2015, **3**, 054006.
22 W. Du, L. Li, K. P. Nichols and R. F. Ismagilov, *Lab Chip*, 2009, **9**, 2286.
23 D. E. Cohen, T. Schneider, M. Wang and D. T. Chiu, *Anal. Chem.*, 2010, **82**, 5707–5717.
24 J.-u. Shim, G. Cristobal, D. R. Link, T. Thorsen, Y. Jia, K. Piattelli and S. Fraden, *J. Am. Chem. Soc.*, 2007, **129**, 8825–8835.
25 W. Shi, J. Qin, N. Ye and B. Lin, *Lab Chip*, 2008, **8**, 1432.
26 J.-u. Shim, L. F. Olguin, G. Whyte, D. Scott, A. Babtie, C. Abell, W. T. S. Huck and F. Hollfelder, *J. Am. Chem. Soc.*, 2009, **131**, 15251–15256.
27 C. H. J. Schmitz, A. C. Rowat, S. Köster and D. A. Weitz, *Lab Chip*, 2009, **9**, 44–49.
28 M. Sun, S. S. Bithi and S. A. Vanapalli, *Lab Chip*, 2011, **11**, 3949.
29 L. Derzsi, *et al.*, *Lab Chip*, 2016, **16**, 893–901.
30 A. Huebner, D. Bratton, G. Whyte, M. Yang, A. deMello, C. Abell and F. Hollfelder, *Lab Chip*, 2009, **9**, 692–698.
31 P. Abbyad, R. Dangla, A. Alexandrou and C. N. Baroud, *Lab Chip*, 2011, **11**, 813–821.
32 J. Pan, A. L. Stephenson, E. Kazamia, W. T. S. Huck, J. S. Dennis, A. G. Smith and C. Abell, *Integr. Biol.*, 2011, **3**, 1043.
33 H. N. Joensson, M. Uhlén and H. A. Svahn, *Lab Chip*, 2011, **11**, 1305–1310.
34 L. Boitard, D. Cottinet, C. Kleinschmitt, N. Bremond, J. Baudry, G. Yvert and J. Bibette, *Proc. Natl. Acad. Sci. U. S. A.*, 2012, **109**, 7181–7186.
35 R. Dangla, S. Kayi and C. Baroud, *Proc. Natl. Acad. Sci. U. S. A.*, 2013, **110**, 853–858.
36 J. Heikenfeld, K. Zhou, E. Kreit, B. Raj, S. Yang, B. Sun, A. Milarcik, L. Clapp and R. Schwartz, *Nat. Photonics*, 2009, **3**, 292–296.
37 R. S. Breed and W. D. Dotterrer, *J. Bacteriol.*, 1916, **1**, 321–331.
38 M. Najah, A. D. Griffiths and M. Ryckelynck, *Anal. Chem.*, 2012, **84**, 1202–1209.
39 B. Vogelstein and K. W. Kinzler, *Proc. Natl. Acad. Sci. U. S. A.*, 1999, **96**, 9236–9241.
40 S. Dube, J. Qin and R. Ramakrishnan, *PLoS One*, 2008, **3**, 1–9.
41 M. H. Zwietering, I. Jongerburger, F. M. Rombouts and K. van't Riet, *Appl. Environ. Microbiol.*, 1990, **56**, 1875–1881.
42 J. Baranyi and C. Pin, *Appl. Environ. Microbiol.*, 1999, **65**, 732–736.
43 C. Guermonprez, S. Michelin and C. N. Baroud, *Biomicrofluidics*, 2015, **9**, 054119.
44 E. Fradet, C. McDougall, P. Abbyad, R. Dangla, D. McGloin and C. N. Baroud, *Lab Chip*, 2011, **11**, 4228–4234.
45 M. L. Ferguson, D. Le Coq, M. Jules, S. Aymerich, N. Declerck and C. A. Royer, *Anal. Biochem.*, 2011, **419**, 250–259.
46 M. L. Cordero, H. O. Rolfsnes, D. R. Burnham, P. A. Campbell, D. McGloin and C. N. Baroud, *New J. Phys.*, 2009, **11**, 075033.
47 J. Baranyi and T. A. Roberts, *Int. J. Food Microbiol.*, 1994, **23**, 277–294.

